ORIGINAL PAPER

Synthesis and characterization of porous activated carbons derived from lotus nut and their performance for CO_2 adsorption

B. Mousazadeh[1] · N. Mohammadi[1] · M. R. Khosravi-Nikou[1]

Abstract

The purpose of the current work is to transform the lotus nut, as a new precursor, into a low-cost, high-performance, porous activated carbon through a one-step chemical activation method using two different activating chemicals, Potassium hydroxide (KOH) and Zinc chloride ($ZnCl_2$) with the objective of the largest surface area, hence the maximum CO_2 adsorption capacity. Response Surface Methodology (RSM) was used to optimize critical production conditions, including the chemical to precursor ratio, activation time, and activation temperature. The largest specific surface area of the Activated Carbon prepared from KOH (ACK) was 1115.32 m^2/g, which was obtained at the activation temperature of 726 °C, activation time of 134 min, and the chemical reagent ratio of 2.78. While, the specific surface area of the Activated Carbon prepared from $ZnCl_2$ (ACZ) was 912.51 m^2/g, which was achieved at 70 min, 653 °C, and 1.74. The maximum CO_2 adsorption capacity of prepared activated carbons at 5 bar under optimal conditions was found to be 4.4 mmol/g for activated carbon prepared using KOH. The Scanning Electron Microscopy (SEM) images indicated that the use of KOH results in deeper and narrower pores, while larger pores were visible for the activated carbon prepared by $ZnCl_2$. The surface of activated carbons includes functional groups that contain nitrogen, according to the Fourier Transform Infrared Spectroscopy (FTIR) analysis.

Graphical abstract
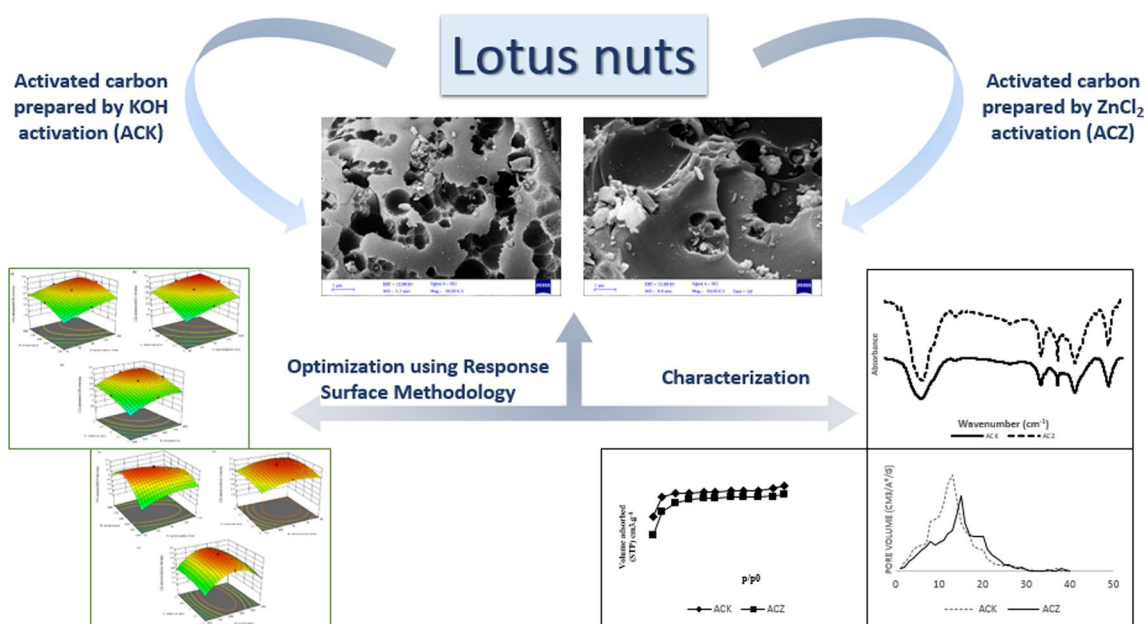
Editorial responsibility: Mohamed F. Yassin.

Extended author information available on the last page of the article

Introduction

Contamination has emerged as a significant worldwide issue, primarily because of their detrimental effects on the well-being of living organisms (Liu et al. 2023; Chang et al. 2022; Yuan et al. 2023). Pollutants are widely distributed due to the swift expansion of industrialization and certain human actions (Liang et al. 2021; Tian et al. 2023; Kan et al. 2023; Zhang et al. 2023a). Among them, the greenhouse effect and air pollution challenges that carbon dioxide causes to the environment make it one of the most significant environmental issues (Li et al. 2022; Chen et al. 2023; Ravi et al. 2022). Several sources discharge carbon dioxide to the atmosphere, such as chemical and petrochemical activities, fossil fuel power plants, and refineries (Cheng et al. 2021; Liu et al. 2022; Li et al. 2023a, 2023b). Eliminating carbon dioxide from air can play a crucial role in decreasing air pollution and global warming (Zhang et al. 2023b; Li et al. 2023a, 2023b; Maniarasu et al. 2022). Multiple methods have been widely used for capturing CO$_2$, including separation with membrane, absorption, and adsorption (Abdelhamid 2022; Gao et al. 2023). Among them, adsorption stands out as a desirable technology that can be developed in industrial scale due to its advantages such as low energy consumption, cost-effectiveness, and applicability over a wide range of pressures and temperatures (Bai et al. 2019; Hajilari et al. 2019). Choosing a satisfactory adsorbent for CO$_2$ adsorption is of high significance. Miscellaneous types of materials have been applied for the CO$_2$ adsorption process, including activated carbon, metal–organic frameworks, polymer-based materials, and zeolites (Mohammadi et al. 2021). However, activated carbon has been mostly recommended as an appealing material for CO$_2$ capturing because of its advantageous characteristics, including large surface area, high porosity, easy and simple manufacturing, availability, and cost benefit (Hajilari et al. 2019). Over the past decades, the most commonly used materials for activated carbon fabrication are organic precursors that are rich in carbon. Therefore, the development of methods to convert used materials into activated carbon is of great interest and provides a promising future (Dong et al. 2022; Zhang et al. 2021; Hu et al. 2022). In this regard, a large number of researches have been recently reported on activated carbon production from biomass derivatives, including barley husks, pistachio shell, nutshells, cotton stalks, wood sawdust, corn cob, bagasse and rice husk (Lua et al. 2004; Medhat et al. 2021; Wang et al. 2023; Nahil and Williams 2012; Osasona et al. 2018; Zhang et al. 2020). The aforementioned materials have been

found proper precursors due to their high strength and hardness in which these features are owing to their high lignin and carbon content (Cagnon et al. 2009; Hernandez et al. 2007). The most frequently used methods to convert bio-wastes to activated carbon are physical and chemical activation (Ayinla et al. 2019; Al-Swaidan and Ahmad 2011). In physical activation method, carbonized material is gasified by oxidizing gases, mostly steam and carbon dioxide, in the temperature range of 800–1000 °C (Mahapatra et al. 2012; Budinova et al. 2006). However, during the chemical activation process, materials are previously impregnated with a chemical (mainly H$_3$PO$_4$, ZnCl$_2$, or KOH) in which chemical reagents act on the precursor being carbonized. Chemical activation can be conducted in two methods, including one-step or two-step activation. The one-step activation refers to subjecting chemically treated biomass precursors to the pyrolysis process for activated carbon production, while the two-step procedure means firstly carbonizing biomass precursors and then chemically treating them before pyrolysis. These two processes result in different pore structures, surface areas, and surface characteristics. The majority of activating reagents are bonded to biomass precursors during the one-step chemical activation process when the linkages in the botanical structure are broken following impregnation. Afterward, when carbonization occurs, due to the consumption of carbon atoms on active sites, the pore structures are developed. The two-step activation method, on the other hand, engages the biomass precursors through initial carbonization to form biochar with hierarchical pore structures because of the release of pyroligneous acids and gases. Some researchers confirmed that the one-stage activation procedure results in larger surface areas and microporosity. Heidari and colleagues revealed that an H$_3$PO$_4$ activating agent was utilized to produce activated carbon from Eucalyptus camaldulensis wood in a one-step activation procedure, giving a large surface area (1218 m^2/g) and pore volume (0.6 cm^2/g) (Heidari et al. 2019). Elmouwahidi et al. investigated the properties of olive-residue activated carbons using a one-step and two-step chemical method, respectively. In comparison to the BET surface area of biochar-derived activated carbons (1295 m^2/g), biomass-derived activated carbons had a higher value (1390 m^2/g) (Elmouwahidi et al. 2017). For activation by means of chemical reagents usually lower temperature range and less activation time is required, indicating the lower energy consumption of the chemical activation process that leads to lower cost for the final product. In addition, larger surface area and higher porosity can be accomplished (Wang and Liu 2017). Recently, many
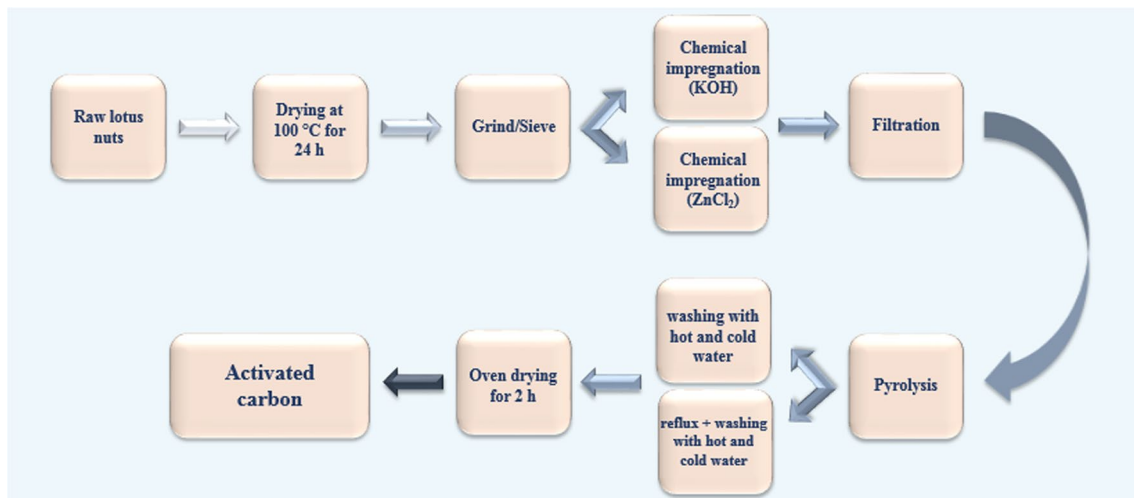
Fig. 1 Activated carbon preparation flow chart

researchers investigated CO_2 capture performance of agricultural waste-based activated carbons. Nagarajan et al. (2022) reported the fabrication of activated carbon derived from agro-waste to investigate CO_2 capture capacity. They found carbon dioxide adsorption capacity reaching 5.225 mmol/g and the surface area of the prepared activated carbon to be 1220 m^2/g. Yokoyama et al. (2019) showed that Stevia residue-based activated carbon has an acceptable surface area and carbon dioxide adsorption uptake of 874 m^2/g and 117 mg/g, respectively. They also optimized activated carbon production conditions, including activation time, CO_2 flow, and activation temperature using Response Surface Methodology. Alhassan et al. (2018) fabricated activated carbon from sugarcane bagasse to explore acid and base modification on CO_2 adsorption capacity. They showed that the activated carbon modified with basic chemicals had the highest adsorption capacity of 148.5 mg/g. Ramesh et al. (2018) used cotton as a new precursor to produce porous activated carbon with satisfactory surface area and large CO_2 uptake of 2.61 mmol/g. He et al. (2021) obtained activated carbon from rice husk to investigate its CO_2 adsorption capacity. They obtained surface area, total pore volume and the maximum CO_2 adsorption capacity of 1495.52 m^2/g, 0.786 cm^3/g and 5.83 mmol/g under optimum condition, respectively. The current work aims to transform agricultural waste, the lotus nut, into a low-cost, high-performance porous activated carbon with the objective of the largest specific surface area, hence maximum CO_2 adsorption capacity. Lotus nut is an agricultural waste found abundantly in Khuzestan province of Iran, which has several merits to use for activated carbon production. Similar to some other biomass wastes, it has high strength and hardness making it suitable for processes with high pressures. According to our previous work, its carbon content (over 60%) is remarkably higher than that of other biomass derivatives resulting in larger yields (Mousazadeh et al. 2021). Usingagricultural waste materials considerably reduces the production cost because the raw material is almost at no cost. One-step chemical activation was selected for the process because it was aimed to achieve the maximum surface, pore volume and the lowest energy consumption. Activated carbons synthesized using $ZnCl_2$ and KOH as activation reagents, and their performance for CO_2 adsorption was evaluated. Response Surface Methodology (RSM) was used to optimize critical production conditions, including the chemical to precursor ratio, activation time, and activation temperature. Moreover, the surface properties of prepared activated carbons were investigated using FT-IR and SEM analysis.

Materials and methods

Reagents

Chemical reagents used in the current study are KOH, $ZnCl_2$, and HCl, which all were purchased from Merck Company and used as received. Lotus nuts were obtained from different parts in Ahwaz, Iran. They were sieved to a size range of 1–2 mm after being dried at 100 °C for one day.

Activated carbon preparation

The production procedure of activated carbon from lotus nut is shown in Fig. 1. To eliminate the initial moisture, lotus nuts were first dried at 100 °C for one day. Dried nuts were sieved to obtain a uniform material with a particle size of 1–2 mm. According to Table 1, 20 samples with different preparation conditions were made. Firstly, the previous

Table 1 Experimental design matrix, corresponding parameters and responses for ACK and ACZ production

Std	Run	Factor 1 A:activation time	Factor 2 B:activation temperature	Factor 3 C:chemical ratio	Response 1 BET surface area(ACK)	Response 2 BET surface area (ACZ)
					m^2/g	m^2/g
11	1	90	500	2	914.39	800.56
9	2	30	650	2	939.89	897.18
18	3	90	650	2	1023.69	925.61
1	4	30	500	1	673.95	738.85
14	5	90	650	3	1071.05	885.01
8	6	150	800	3	1113.26	653.6
10	7	150	650	2	1081.97	856.58
4	8	150	800	1	958.11	669.83
6	9	150	500	3	994.54	775.39
20	10	90	650	2	1020.04	921.54
3	11	30	800	1	819.67	824.10
7	12	30	800	3	987.25	779.45
12	13	90	800	2	1030.97	787.57
19	14	90	650	2	1020.04	909.36
13	15	90	650	1	918.03	885.01
15	16	90	650	2	1009.11	921.54
16	17	90	650	2	1005.47	933.71
5	18	30	500	3	848.81	710.43
2	19	150	500	1	834.24	803.80
17	20	90	650	2	1030.97	913.42

material were originally treated with a saturated mixture of the chemical reagent (KOH or ZnCl$_2$) at a mass ratio of 1–3. To do this, four grams of the precursor was added to 50 mL deionized water and chemical reagents were introduced to the mixture at amounts of 4, 8, and 12 gr. For 24 h, the mixture was agitated at room temperature, while maintaining a nearly constant volume of solution. After that, the pretreated sample was filtered and heated for two hours. Following that, the sample was heated in a tubular horizontal furnace under a N$_2$ gas flow for 30, 90, and 150 min time intervals to achieve a temperature of 500, 650, 800 °C (heating rate 5 °C/min). After carbonization, the samples were thoroughly subjected to washing with hot and cold deionized water to eliminate any remaining chemicals. The extra refluxing step was performed before subjecting to washing for the carbonaceous material impregnated with ZnCl$_2$, in order to completely eliminate chemical reagent residual. Activated carbons impregnated with KOH and ZnCl$_2$ are expressed as ACK and ACZ, respectively, along with the text.

Experimental design

It is necessary to limit the number of experiments due to the high expense of research (Lu et al. 2022). RSM is an appropriate strategy for modeling and process optimization when numerous independent factors impact a response of interest (Roosta et al. 2014). The design of experiments was constructed using RSM in Central Composite Design (CCD) space. According to previous research works, the most important process variables for activated carbon production from biomass waste are activation time, activation temperature, and chemical to precursor ratio (Mousazadeh et al. 2021). Therefore, independent variables chosen for the current work are activation time (A), activation temperature (B), and chemical ratio (C), where each factor has three levels (low, center, high). The experiment layout was set after applying the level of variables and the test domain, and 20 runs were generated. The complete design and corresponding parameters, as well as the experimental domain and level of variables, are summarized in Tables 1 and 2. The following quadratic polynomial model was

Table 2 Level of variables and experimental domain for activated carbon production

Variable	Low	High	− alpha	+ alpha
Activation time (min)	30	150	30	150
Activation temperature (°C)	500	800	500	800
Chemical ratio (g/g)	1	3	1	3

selected for the anticipation of the mathematical relationship between process variables and the corresponding responses (Hajati et al. 2014).

$$Y = \beta 0 + \sum_{i=1}^{k} \beta_i X_i + \sum_{i=1}^{k} \beta_{ii} X_i^2 + \sum_{i=1}^{k-1} \sum_{j=2}^{k} \beta_{ij} X_i X_j \qquad (1)$$

where y refers to the predicted response, X_i to X_j coded variables, β_0 denotes the constant coefficient, β_i is the linear term coefficients, β_{ij} is the quadratic coefficients, and k is the number of variables that are involved in the activated carbon preparation. The analysis of variance (ANOVA) was used to determine the statistical significance of each term as well as the developed models.

Results and discussion

Statistical study

The impact of three independent variables of activated carbon production conditions, such as activation time (A), activation temperature (B), and chemical to precursor ratio (C), was investigated based on CCD, the overall design, as well as BET surface area results, are illustrated in Table 1. Both ACZ and ACK exhibited a high BET surface area; however, better results were obtained for ACK. By applying several regressions, the mathematical correlation between surface area and the preparation variables of activated carbons were found to be a polynomial quadratic model for both adsorbents. The results of obtained models in terms of ANOVA for both adsorbents are shown in Tables 3 and 4. Calculated

Table 3 Analysis of variance for ACK

Source	Sum of squares	df	Mean square	F-value	p-value	
Model	2.107E+05	9	23,413.27	192.11	<0.0001	Significant
A-activation time	50,771.45	1	50,771.45	416.59	<0.0001	
B-activation temperature	41,386.38	1	41,386.38	339.58	<0.0001	
C-chemical ratio	65,756.59	1	65,756.59	539.55	<0.0001	
AB	216.08	1	216.08	1.77	0.2126	
AC	91.16	1	91.16	0.7480	0.4074	
BC	19.32	1	19.32	0.1585	0.6989	
A^2	1224.20	1	1224.20	10.04	0.0100	
B^2	9687.07	1	9687.07	79.48	<0.0001	
C^2	3865.68	1	3865.68	31.72	0.0002	
Residual	1218.74	10	121.87			
Lack of fit	774.14	5	154.83	1.74	0.2788	Not significant
Pure error	444.59	5	88.92			
Cor total	2.119E+05	19				

Table 4 Analysis of variance for ACZ

Source	Sum of squares	Df	Mean square	F-value	p-value	
Model	1.482E+05	9	16,465.67	127.93	<0.0001	Significant
A-activation time	3640.69	1	3640.69	28.29	0.0003	
B-activation temperature	1310.64	1	1310.64	10.18	0.0096	
C-chemical ratio	1386.06	1	1386.06	10.77	0.0083	
AB	21,015.51	1	21,015.51	163.28	<0.0001	
AC	100.95	1	100.95	0.7843	0.3966	
BC	2.06	1	2.06	0.0160	0.9018	
A^2	2993.71	1	2993.71	23.26	0.0007	
B^2	36,884.20	1	36,884.20	286.57	<0.0001	
C^2	1701.59	1	1701.59	13.22	0.0046	
Residual	1287.09	10	128.71			
Lack of fit	910.77	5	182.15	2.42	0.1771	Not significant
Pure error	376.32	5	75.26			
Cor total	1.495E+05	19				

P and F values were evaluated to assess the significance of each variable. Model terms are considered significant when the P-value is less than 0.0500 and the F-value is large (Demim et al. 2014). Therefore, the model terms A, B, C, A^2, B^2, C^2 with low p-values are significant for ACK. Similar terms were appeared to have the most significant impact on the surface area of ACZ; in this case, A^2, B^2, C^2, AB, A, B, and C are important parameters of the constructed model. According to F and p values displayed in Tables 3 and 4, the relationship between activated carbon synthesis conditions and BET surface area is significant for both adsorbents revealing the high conformance of constructed models for prediction of preparation results. The lack of fit values, however, for ACK and ACZ were calculated to be 1.74 and 2.42, respectively, and are not statistically significant. In addition, the comparison between predicted R^2 values ($R^2_{pre} = 0.9796$ and $R^2_{pre} = 0.9485$ for ACK and ACZ, respectively) and adjusted R^2 values ($R^2_{adj} = 0.9891$ and $R^2_{adj} = 0.9836$ for ACK and ACZ, respectively) as well as the coefficients of determination ($R^2 = 0.9942$ and $R^2 = 0.9914$ for ACK and ACZ, respectively) clearly convey the satisfactory agreement of actual data with those predicted by the models (Table 5). Therefore, it can be deduced that the constructed models were well fitted with the experimental data. The linear plots of predicted responses versus actual ones are presented in Fig. 2a, b. These plots with high coefficients of determina-

4 as a function of two independent variables, while the other variables are at the fixed level. According to ANOVA results presented in Tables 3 and 4, activation time was appeared to have the most impact on the specific surface area of ACZ while activation temperature and chemical impregnation ratio showed less impact. The quadratic function of chemical ratio and activation time exhibited a similar effect on the surface area of ACZ. In contrast, the quadratic function of activation temperature had an appreciable impact on surface area (due to the largest F value of 286.57 between quadratic functions). It is obvious that the interaction between activation temperature and activation time has the largest impact on the S_{BET} of ACZ. In the case of ACK, on the other hand, activation time and activation temperature demonstrated a great impact on the surface area, and the highest effect was observed for chemical ratio with the largest F value of 539.55. The square terms of variables, however, owing to lower F values, exhibited less impact on the surface area of ACK. Activated carbons under optimal conditions are presented in Table 6.

Activation temperature versus activation time

The parallel impact of activation time and activation temperature on the process at a constant chemical ratio of 2 is shown in Figs. 3a and 4a. Figure 4a shows that when the activation temperature was increased, the surface area

Table 5 Model summary statistics

	Std. Dev	Mean	C.V. %	R^2	Adjusted R^2	Predicted R^2	Adeq precision
ACK	11.04	964.78	1.14	0.9942	0.9891	0.9796	55.5140
ACZ	11.34	829.63	1.37	0.9914	0.9836	0.9485	32.9329

tion satisfactorily confirm the aforementioned explanations. The ultimate models in terms of variables which had the most impact on specific surface area are presented as follows (Eqs. (1)–(2)):

$$Y_1 = 2.81 + 0.1950A + 0.1760B + 0.2220C - 0.0582A^2 - 0.1632B^2 - 0.1032C^2 \tag{2}$$

$$Y_2 = 2.26 - 0.0470A - 0.0282B - 0.0290C - 0.1262AB - 0.0813A^2 - 0.02853B^2 - 0.0613C^2 \tag{3}$$

Effect of preparation variables on the BET surface area

The combined impact of activation time (A), activation temperature (B), and chemical ratio (C) on the specific surface area of adsorbents were investigated using response surface methodology (RSM). The 3D plots are shown in Figs. 3 and

was dramatically enhanced and an additional increase in the activation temperature resulted in a decrease in the specific surface area. A similar result was obtained for ACK at a temperature of 500–650 °C, followed by a slight decrease in surface area at activation temperatures larger than 650 °C. The positive effect of lower temperatures can be perceived by the development of the pore structure of ACs because of the release of volatiles from the matrix during carbonization. In comparison, the reduction of specific surface area at higher temperatures can be the result of the widening of micropores and the formation of mesopores and macropores (Ahmad and Alrozi 2010; Ip et al. 2008).

Activation temperature versus chemical ratio

The parallel impact of activation temperature and chemical to precursor ratio on the BET surface area at constant activation time of 90 min is conveyed in Figs. 3c and 4c. For ACZ, the increase in chemical ratio and activation temperature
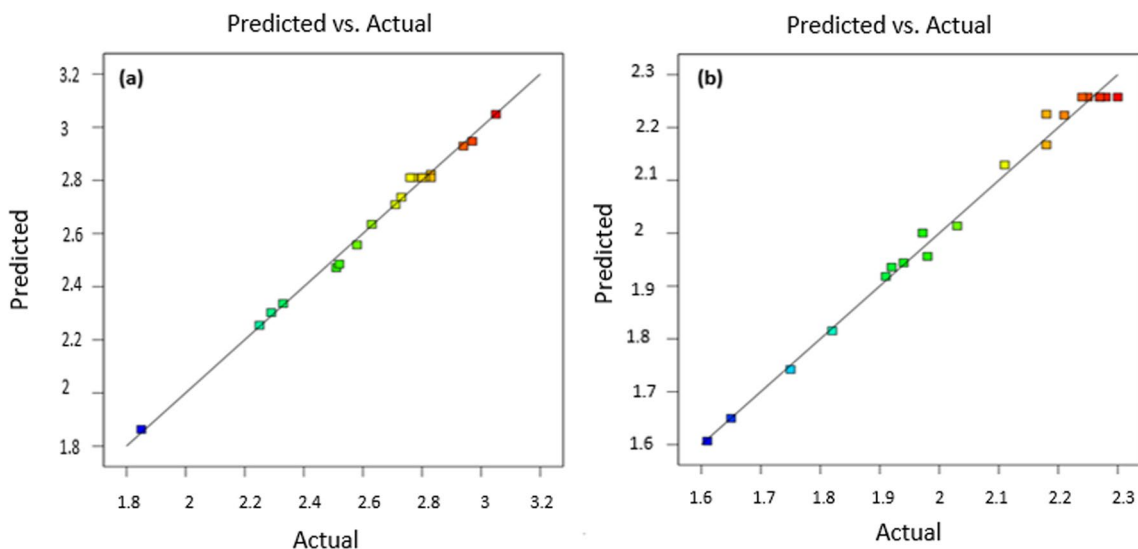
Fig. 2 **a** Predicted values vs actual data for ACK, **b** Predicted values vs actual data for ACZ
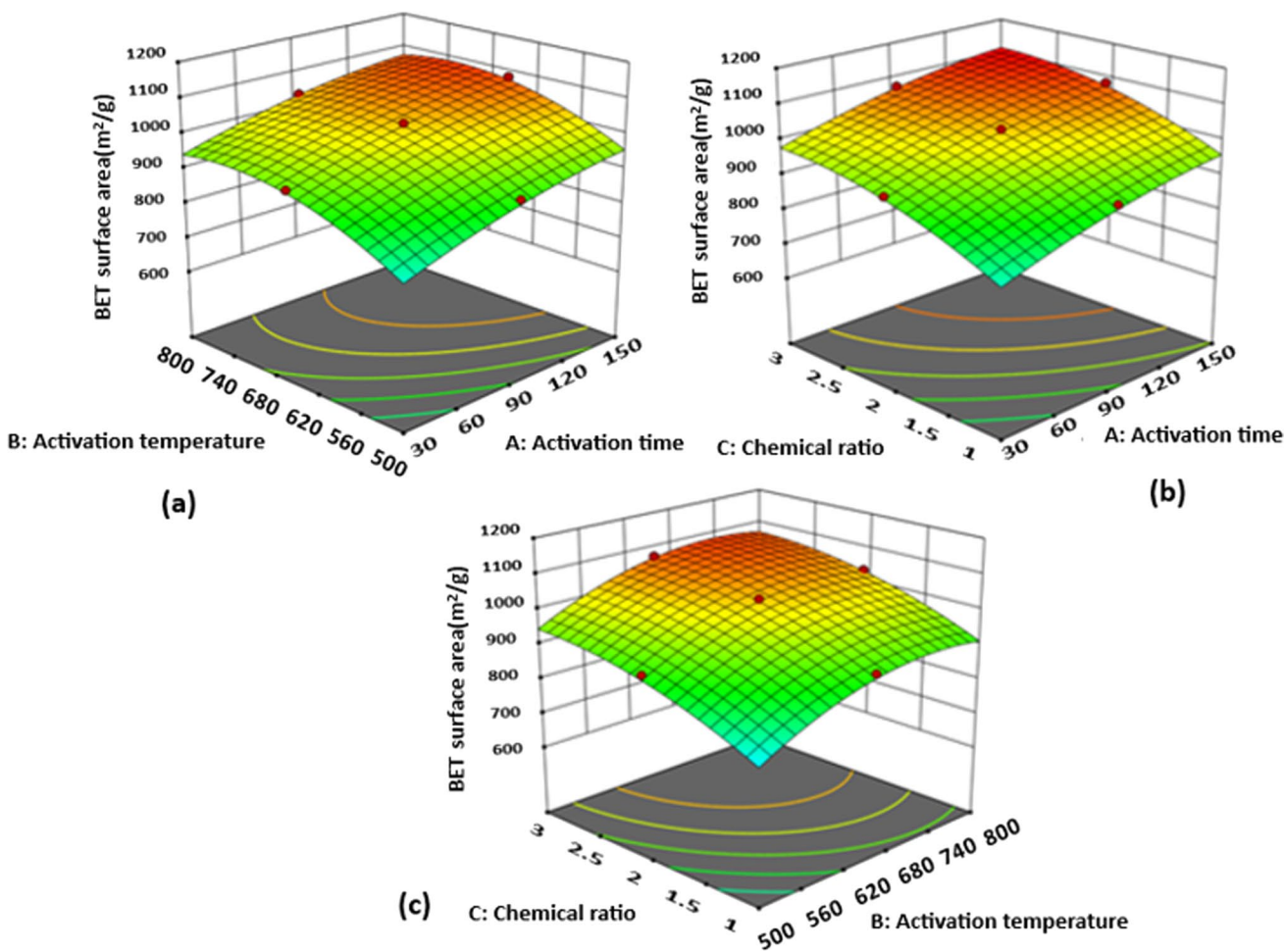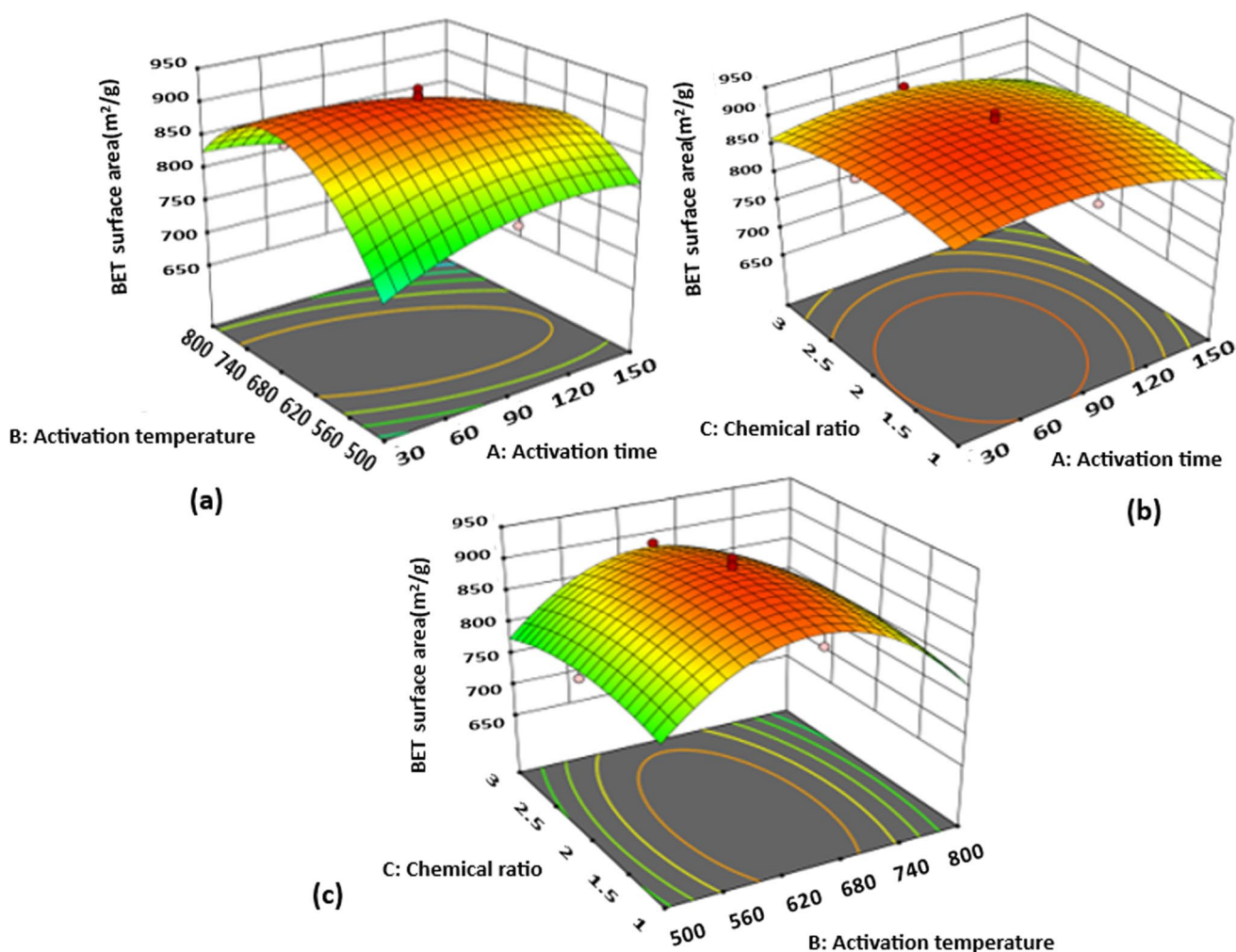

Fig. 3 Three-dimensional plots of the effect of activated carbon ACK preparation variables on BET surface area

Fig. 4 Three-dimensional plots of the effect of activated carbon ACZ preparation BET surface area

Table 6 Textural properties of activated carbons under optimal conditions

Adsorbent	S_{BET} (m²/g)	Total pore volume (cm³/g)	Micropore volume (cm³/g)	Average pore width (Å)
ACK	1115.32	0.545	0.397	19.21
ACZ	912.51	0.487	0.326	20.12

promotes an enhancement in the surface area, while the high level of activation temperature and chemical ratio negatively impact the specific surface area. This could be the result of deterioration of pore structure and the extensive burn-off of carbon content that unfavorably influenced the quality of pores (Gratuito et al. 2008). On the other hand, for ACK, by increasing activation temperature and chemical ratio surface area of the adsorbent improved. At high levels of chemical ratio and activation temperature, responses tend to increase even at levels greater than experimental design. The higher

level of chemical ratio and activation temperature can have a positive effect on the promotion of pore networks; however, it means the higher consumption of chemicals and energy, which is a disadvantage from an economic point of view. The proposed mechanism for the KOH activation process consists of three main stages. The first region pertains to the carbon gasification and the formation of potassium oxide, which occurs in the temperature range of 80–250 °C, the possible reactions are stated in Eqs. (4–6). Consumption of carbon atoms on active sites due to the gasification reaction leads to the development of pore structure. The second stage is related to the formation of potassium carbonates between 250 and 680 °C, as represented in Eq. (7). The final stage takes place at a temperature range higher than 680 °C, as shown in Eqs. (8–10). At this stage, the reduction of K_2O by hydrogen or carbon atoms leads to the promotion of greater microporosity and higher surface area (Alhamed et al. 2015; Parshetti et al. 2015; Tan et al. 2015). In fact, most of the micropore networks are generated at this stage, where the

depletion of carbons during K_2O reduction leaves a void space that contributes to the development of microporosity (Wang et al. 2012). Also, the metallic potassium formed from the reduction of K_2O alters from solid to vapor phase, the potassium vapor passes through carbon lattices that leads to the formation of pore structures. Another possible reaction that seldom occurs during the activation process is stated in Eq. (10) (Li et al. 2017).

$$2KOH \rightarrow K_2O + H_2O \tag{4}$$

$$C + H_2O \rightarrow CO + H_2 \tag{5}$$

$$CO + H_2O \rightarrow CO_{2+}H_2 \tag{6}$$

$$K_2O + CO_2 \rightarrow K_2CO_3 \tag{7}$$

$$K_2CO_3 \rightarrow K_2O + CO_2 \tag{8}$$

$$K_2O + H_2 \rightarrow 2K + H_2O \tag{9}$$

$$K_2O + C \rightarrow 2K + CO \tag{10}$$

Chemical ratio versus activation time

The impact of activation duration and chemical ratio on the surface area at a constant activation temperature of 650 °C is shown in Fig. 4b, c. The surface area of ACZ was slightly increased by increasing activation time. However, longer duration caused a moderate reduction in the surface area. Figure 4b shows that prolonged activation time resulted in an increase in the specific surface area. Even though a lengthy time interval may result in a huge surface area, it is not financially viable since the high activation temperature must be kept for an extended period of time.

Process optimization

A numerical optimization approach based on RSM was used to improve the activated carbon production parameters with the goal of maximizing the surface area. The optimal conditions for ACK were activation temperature of 726 °C, activation time of 134 min, and the chemical reagent ratio of 2.78. However, these optimum conditions were 70 min, 653 °C, and 1.74 for ACZ. In addition, the maximum surface area was found to be 1117.94 and 920.92 m^2/g for ACK and ACZ, respectively. To explore the validation of the optimization process, activated carbons were prepared under optimum settings. The surface area of the fabricated activated carbons under optimum preparation conditions was appeared to be 1115.32 m^2/g and 912.51 m^2/g for ACK and ACZ, respectively. The specific surface area obtained at optimum conditions matched well with the predicted responses obtained from the constructed models. Table 7 includes an overview of activated carbons derived from other biomass wastes. According to this table, the specific surface area obtained for the as-synthesized activated carbons shows that lotus nut has promising potential for activated carbon production. For instance, the surface area obtained for ACK and ACZ was larger than that of rice husk, garlic peel, and coconut shell. Considering the abundance of lotus nut in Iran, its high strength and hardness, large CO_2 adsorption capacity, and high carbon content, it is clear that lotus nut can be assigned as a new alternative for activated carbon production with large surface areas.

Characterization

Due to a large number of adsorbent samples, the BET analysis as well as textural properties, including average pore width, surface area, and total pore volume were only reported under optimal conditions. Also, the structural properties of ACK and ACZ prepared under optimum conditions were analyzed using FTIR spectroscopy and SEM methods.

Table 7 An overview of other activated carbons derived from agricultural waste

Precursor	Chemical activation reagent	Specific surface area (m^2/g)	Reference
Oil palm shell	$ZnCl_2$	1118	Arami-Niya et al. (2011)
Palm Kernel Shell	$ZnCl_2$	953	Hidayu and Muda (2016)
Coconut shell	$ZnCl_2$	251	Ahmed et al. (2017)
Kanlow Switchgrass	KOH	1272	Oginni et al. (2019)
Garlic peel	KOH	947	Huang et al. (2019)
Rice husk	$ZnCl_2$	749	Raut et al. (2022)
Lotus nut	KOH/$ZnCl_2$	1115.32/912.51	Current work

Fig. 5 N$_2$ adsorption–desorption of ACK and ACZ, pore size distribution of ACK and ACZ
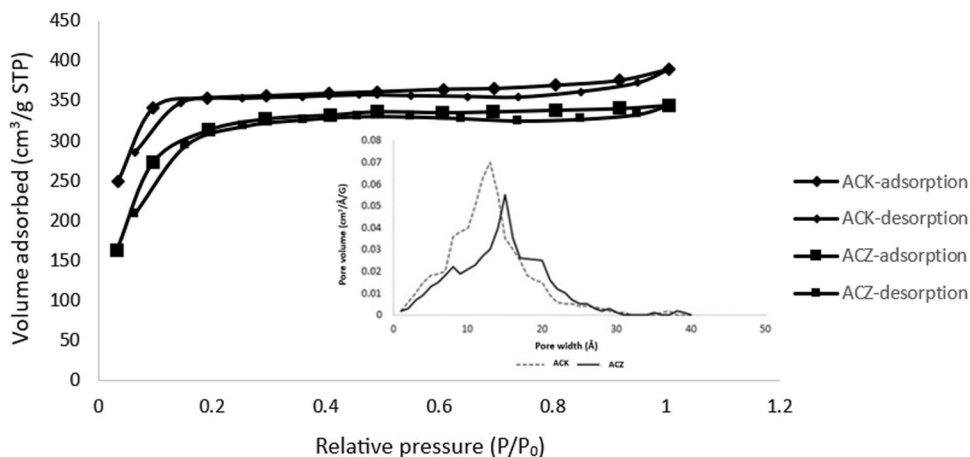
BET analysis

The N$_2$ adsorption isotherms of both ACK and ACZ samples prepared at optimum conditions are displayed in Fig. 5. The shape of both isotherms is very similar. According to IUPAC classifications, the isotherms might be categorized as type I isotherm. As can be seen from Fig. 5, for both types of adsorbents, adsorption of nitrogen molecules mostly takes place in the low-pressure range ($p/p_0 < 0.2$) while at higher relative pressures, nitrogen gas adsorption tends to level off and is rather small. The existence of large adsorption capacity at low relative pressures followed by a limiting value indicated by the plateau at relative pressures above 0.2 is due to the higher volume of narrow pores, particularly micropores, that they cannot accommodate more than a single molecular layer. Although both samples exhibit type I isotherm, ACK shows a higher volume of N$_2$ adsorption in comparison with ACZ. For ACZ, the presence of a wider adsorption knee indicates the contribution of wider micropores and small mesopores in adsorption of nitrogen molecules, while for ACK, there is less increase in adsorption capacity at higher relative pressures indicating that the nitrogen molecules mostly adsorbed in micropores. Figure 5 also conveys the difference in the pore size distribution of ACK and ACZ. According to this figure, the pore structure of ACK is mostly dominated by micropores with pore width less than 15 Å. However, ACZ exhibits more volume of pores at pore width ranging between 10 and 20 Å. The generation of larger micropores in ACZ is due to acid attack mechanism of ZnCl$_2$ activation process in which chemical agent acts as an acid catalyst leading to bond cleavage reactions and destruction of the botanical structure of precursor (Yahya et al. 2015). However, using KOH as a chemical reagent makes it possible to tailor the pore structure more accurately with narrower pore distribution. Both activating reagents assist specific surface area enlargement, KOH having more impacts on creating micropores and increasing specific surface area. Some textural properties, including average pore width average pore width, surface area, and total pore volume are also recorded in Table 6. High pore volume and surface area are obtained for ACK and ACZ under optimal preparation conditions.

FTIR analysis

The surface characteristic of activated carbons was analyzed using FTIR spectroscopy. The FTIR spectra of both ACK and ACZ under optimum preparation conditions are presented in Fig. 6. The IR spectra graphs of both samples exhibit almost similar results. The broad and intense peaks around 3430 cm^{-1} are attributed to the O–H stretching vibrations of hydroxyl groups or the existence of (N–H) amine groups (Shafeeyan et al. 2010). The presence of bands at 1620 cm^{-1} is derived from alkene (C=C) or amide groups (Shafeeyan et al. 2010; Guo and Lua 2003). The peaks observed at 1385 cm^{-1} are attributed to the bending of C–H group (Yakout and El-Deen 2016). Peaks around 1120 cm^{-1} are attributed to C–O and C–N bonds (Shafeeyan et al. 2010). Also, peaks around 620 cm^{-1} correspond to aromatic C–H groups (Yakout and El-Deen 2016). As the FTIR results show, nitrogen-containing functionalities may exist on the surface of activated carbons. These groups help to increase the surface basicity of activated carbons making the surface of activated carbons suitable for CO$_2$ adsorption (Plaza et al. 2009).

SEM analysis

SEM method was used to investigate the surface morphology of produced activated carbons under optimal preparation conditions (Fig. 7). SEM images illustrate the porous structure of both ACK and ACZ. Heterogeneous and irregular
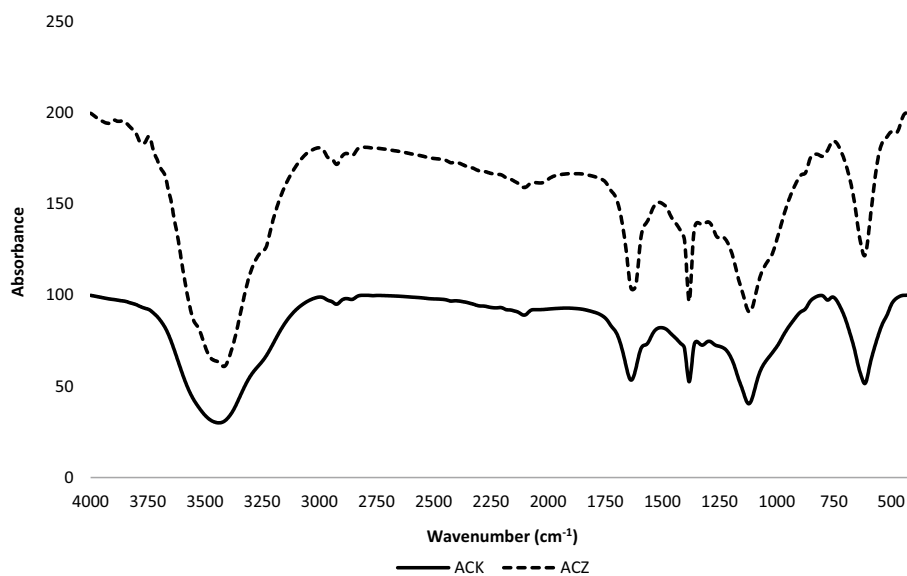
pore structure with channel-like shapes can be observed for both samples. ACK exhibits a higher number of pores than ACZ, hence higher surface area was obtained for ACK. In the sample activated with KOH, the formation of narrower and deeper pore network is also visible. However, larger pores exist on the surface of ACZ; it can be due to the degradation of the botanical structure of precursor, leaving empty spaces that contribute to the porosity of the activated carbon. The presence of small white particles may be related to chemical reagents residual.

CO2 Adsorption isotherms

The capability of prepared activated carbons for CO_2 adsorption was investigated under room temperature condition. A manometric adsorption apparatus was used to perform the CO_2 adsorption procedure, which is schematically shown in Fig. 8. The activated carbons were degassed overnight in a vacuum oven at 180 °C. They were then immediately moved to the adsorption cell to perform the adsorption test. The experimental conditions for CO_2 adsorption test were a pressure range of 0–5 bar, the adsorbent dose of 0.1 g, and room temperature (27 °C). The corresponding adsorption isotherms are recorded in Fig. 9. According to this figure, the adsorption capacity increases with increasing pressure. There is a steep increase in the CO_2 adsorption capacity onto ACK at pressures lower than 1 bar following by a slight improvement over 1–5 bar pressure range. The sharp increase below atmospheric pressure indicates that CO_2 molecules, firstly, occupied micropores of the ACK, and then multilayer adsorption occurred in wider micropores and mesopores at higher pressures. The isotherm shape of the ACZ is slightly different. There is a wide adsorption knee in the sub-atmospheric region following by a significant

increase at pressures above 1 bar. The wider adsorption knee at a pressure of 0–2 bar indicates the contribution of wide micropores and narrow mesopores in the CO_2 adsorption. The existence of a dramatic increase in adsorption capacity above atmospheric pressure indicates the presence of multilayer adsorption in mesopores and wide micropores.

Conclusion

The present work illustrated the fabrication of activated carbons from lotus nuts via a one-step chemical activation method using KOH (ACK) and $ZnCl_2$ (ACZ) as chemical activating reagents. RSM was successfully employed to optimize the most important activated carbon preparation conditions. Quadratic polynomial models were obtained to describe the mathematical correlation between BET surface area and variables influencing activated carbon production. The optimum preparation conditions for ACK were obtained to be activation temperature of 726 °C, activation time of 134 min, and the chemical reagent ratio of 2.78. However, optimum variables for ACZ preparation were 70 min, 653 °C, and 1.74. The largest specific surface area achieved at optimum preparation conditions was 1115.32 m^2/g and 912.51 m^2/g for ACK and ACZ, respectively. The SEM images indicated that the use of KOH as an activating agent results in deeper and narrower pores, while larger pores were visible for the activated carbon prepared by $ZnCl_2$. The FTIR analysis revealed that the nitrogen-containing functional groups exist on the surface of prepared activated carbons. Also, the obtained results showed the excellent capability of prepared activated carbons for CO_2 adsorption. One area that requires further research is the optimal feedstock selection for activated
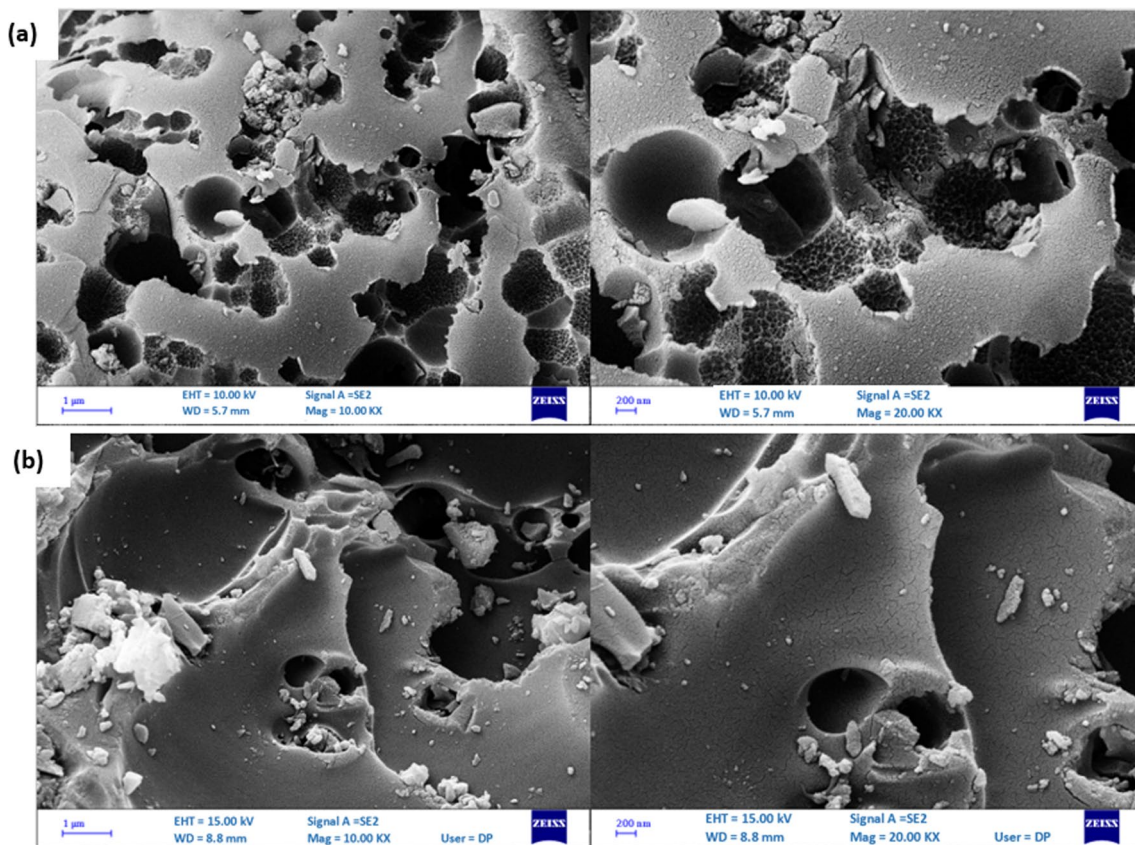
Fig. 7 **a** SEM images of ACK on the scale of 1 μm (left) and 200 nm (right). **b** SEM images of ACZ on the scale of 1 μm (left) and 200 nm (right)
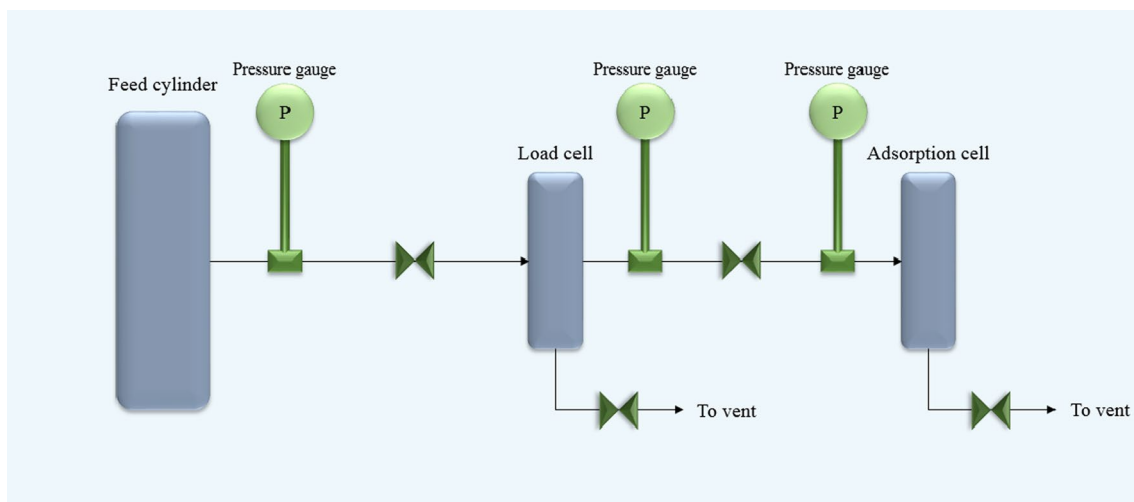

Fig. 8 Schematic diagram of manometric adsorption apparatus

carbon production. Different types of agricultural waste have varying properties, which can affect the effectiveness of the process. For example, the size and shape of the material, as well as its elemental composition, can influence porosity formation during activation. Additionally, the complexity of the manufacturing process can be reduced if the feedstock is chosen based on its material

Fig. 9 Adsorption isotherms of CO_2 gas onto ACK and ACZ
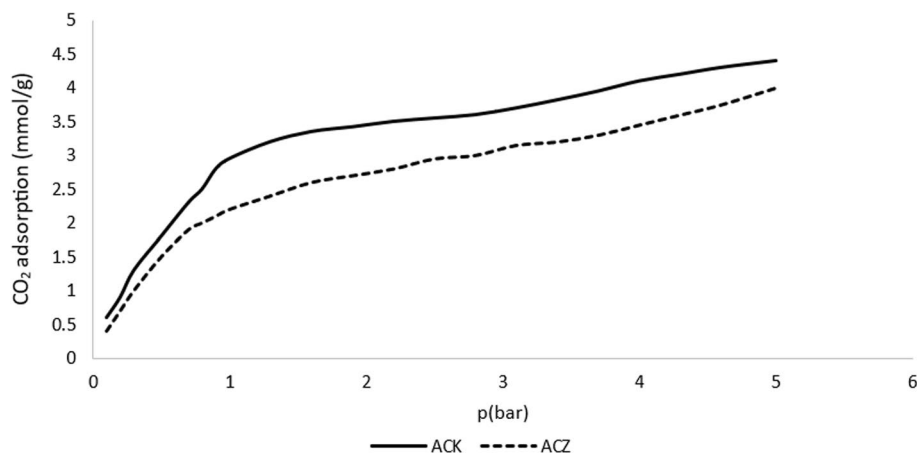
properties. Further research is also needed to optimize the production process. The end product should be of high quality, and the process should be cost-effective. Optimizing the production process can involve improving the efficiency of the activation, introducing new catalysts, or increasing the yield during the process. Investigation of the heating process including microwave and traditional furnace heating considering the high energy demand of traditional tube furnaces is also of significant importance in optimizing the production process. With the right approach, activated carbon production from agricultural waste can become a more viable and cost-effective alternative to traditional activated carbon production.

Data availability The authors of the current study confirm that the data supporting the outcomes of this research are included within the manuscript. Raw data supporting the outcomes of this research are accessible upon reasonable request from the corresponding author.

References

Abdelhamid HN (2022) Removal of carbon dioxide using zeolitic imidazolate frameworks: adsorption and conversion via catalysis. Appl Organomet Chem 36:e6753. https://doi.org/10.1002/aoc.6753

Ahmad MA, Alrozi R (2010) Optimization of preparation conditions for mangosteen peel-based activated carbons for the removal of Remazol Brilliant Blue R using response surface methodology. Chem Eng J 165:883–890. https://doi.org/10.1016/j.cej.2010.10.049

Ahmed S, Mada VV, Kamath V, Jeppu GP (2017) Characterization of activated carbon prepared from coconut shell using various reagents for a low cost water-filter. Int J Eng Technol 9:180–188. https://doi.org/10.21817/ijet/2017/v9i3/170903S029

Alhamed YA, Rather SU, El-Shazly AH, Zaman SF, Daous MA, Al-Zahrani AA (2015) Preparation of activated carbon from fly ash and its application for CO 2 capture. Korean J Chem Eng 32:723–730. https://doi.org/10.1007/s11814-014-0273-2

Alhassan M, Andrew I, Auta M, Umaru M, Garba MU, Isah AG, Alhassan B (2018) Comparative study of CO_2 capture using acid and base modified activated carbon from sugarcane bagasse. Biofuels 9:719–728. https://doi.org/10.1080/17597269.2017.1306680

Ayinla RT, Dennis J, Zaid H, Sanusi Y, Usman F, Adebayo L (2019) A review of technical advances of recent palm bio-waste conversion to activated carbon for energy storage. J Clean Prod 229:1427–1442. https://doi.org/10.1016/j.jclepro.2019.04.116

Al-Swaidan HM, Ahmad A (2011) Synthesis and characterization of activated carbon from Saudi Arabian dates tree's fronds wastes. In: Proc 3rd International conference on chemical, biological and environmental engineering, pp 25–31

Arami-Niya A, Daud WMAW, Mjalli FS (2011) Comparative study of the textural characteristics of oil palm shell activated carbon produced by chemical and physical activation for methane adsorption. Chem Eng Res Des 89:657–664. https://doi.org/10.1016/j.cherd.2010.10.003

Bai B, Rao D, Chang T, Guo Z (2019) A nonlinear attachment-detachment model with adsorption hysteresis for suspension-colloidal transport in porous media. J Hydrol 578:124080. https://doi.org/10.1016/j.jhydrol.2019.124080

Budinova T, Ekinci E, Yardim F, Grimm A, Björnbom E, Minkova V, Goranova M (2006) Characterization and application of activated carbon produced by H3PO4 and water vapor activation. Fuel Process Technol 87:899–905. https://doi.org/10.1016/j.fuproc.2006.06.005

Cagnon B, Py X, Guillot A, Stoeckli F, Chambat G (2009) Contributions of hemicellulose, cellulose and lignin to the mass and the porous properties of chars and steam activated carbons from various lignocellulosic precursors. Bioresour Technol 100(1):292–298. https://doi.org/10.1016/j.biortech.2008.06.009

Chang T, Wang Y, Wang Y, Zhao Z, Shen Z, Huang Y, Veerapandian SKP, Geyter ND, Wang C, Chen Q, Morent R (2022) A critical review on plasma-catalytic removal of VOCs: catalyst development, process parameters and synergetic reaction mechanism. Sci Total Environ 828:154290. https://doi.org/10.1016/j.scitotenv.2022.154290

Chen X, Lv S, Kang J, Wang Z, Guo T, Wang Y, Teobaldi G, Liu LM, Guo L (2023) Efficient C-N coupling in the direct synthesis of urea from CO2 and N2 by amorphous SbxBi1-xOy clusters. Proc Natl Acad Sci. https://doi.org/10.1073/pnas.2306841120

Cheng Z, Guo Z, Fu P, Yang J, Wang Q (2021) New insights into the effects of methane and oxygen on heat/mass transfer in reactive porous media. Int Commun Heat Mass Transf 129:105652. https://doi.org/10.1016/j.icheatmasstransfer.2021.105652

Demim S, Drouiche N, Aouabed A, Benayad T, Couderchet M, Semsari S (2014) Study of heavy metal removal from heavy metal mixture using the CCD method. J Ind Eng Chem 20:512–520. https://doi.org/10.1016/j.jiec.2013.05.010

Dong Y, Yuan H, Ge D, Zhu N (2022) A novel conditioning approach for amelioration of sludge dewaterability using activated carbon strengthening electrochemical oxidation and realized mechanism. Water Res 220:118704. https://doi.org/10.1016/j.watres.2022.118704

Elmouwahidi A, Bailón-García E, Pérez-Cadenas AF, Maldonado-Hódar FJ, Carrasco-Marín F (2017) Activated carbons from KOH and H3PO4-activation of olive residues and its application as supercapacitor electrodes.Electrochim Acta 229:219–228. https://doi.org/10.1016/j.electacta.2017.01.152

Gao S, Zhang Q, Su X, Wu X, Zhang X, Guo Y, Li Z, Wei J, Wang H, Zhang S, Wang J (2023) Ingenious artificial leaf based on covalent organic framework membranes for boosting CO$_2$ photoreduction. J Am Chem Soc 145(17):9520–9529. https://doi.org/10.1021/jacs.2c11146

Gratuito MKB, Panyathanmaporn T, Chumnanklang R-A, Sirinuntawittaya N, Dutta A (2008) Production of activated carbon from coconut shell: optimization using response surface methodology. Bioresour Technol 99:4887–4895. https://doi.org/10.1016/j.biortech.2007.09.042

Grycova B, Pryszcz A, Matejova L, Lestinsky P (2018) Influence of activating reagents on the porous structure of activated carbon. Chem Eng Trans 70:1897–1902. https://doi.org/10.3303/CET1870317

Hajati S, Ghaedi M, Karimi F, Barazesh B, Sahraei R, Daneshfar A (2014) Competitive adsorption of Direct Yellow 12 and Reactive Orange 12 on ZnS: Mn nanoparticles loaded on activated carbon as novel adsorbent. J Ind Eng Chem 20:564–571. https://doi.org/10.1016/j.jiec.2013.05.015

Hajilari M, Shariati A, Khosravi-Nikou M (2019a) Equilibrium and dynamic adsorption of bioethanol on activated carbon in the liquid phase. Chem Eng Technol 42:343–354. https://doi.org/10.1002/ceat.201800219

Hajilari M, Shariati A, Khosravi-Nikou M (2019b) Mass transfer determination of ethanol adsorption on activated carbon: kinetic adsorption modeling. Heat Mass Transf. https://doi.org/10.1007/s00231-019-02575-4

Hamzah Y, Umar L (2017) Preparation of creating active carbon from cigarette filter waste using microwave-induced KOH activation. JPCS. https://doi.org/10.1088/1742-6596/853/1/012027

Heidari A, Khaki E, Younesi H, Lu HR (2019) Evaluation of fast and slow pyrolysis methods for bio-oil and activated carbon production from eucalyptus wastes using a life cycle assessment approach. J Clean Prod 241:118394. https://doi.org/10.1016/j.jclepro.2019.118394

Ji H, Kazehaya A, Muroyama K, Watkinson AP (2000) Preparation of activated carbon from lignin by chemical activation. Carbon 38:1873–1878. https://doi.org/10.1016/S0008-6223(00)00027-0

He S, Chen G, Xiao H, Shi G, Ruan C, Ma Y, Dai H, Yuan B, Chen X, Yang X (2021) Facile preparation of N-doped activated carbon produced from rice husk for CO2 capture. J Colloid Interface Sci 582:90–101. https://doi.org/10.1016/j.jcis.2020.08.021

Hidayu A, Muda N (2016) Preparation and characterization of impregnated activated carbon from palm kernel shell and coconut shell for CO2 capture. Procedia Eng 148:106–113. https://doi.org/10.1016/j.proeng.2016.06.463

Hernandez JR., Aquino FL, Capareda SC (2007) Activated carbon production from pyrolysis and steam activation of cotton gin trash. In: Proc., ASABE annual meeting, p 1. https://doi.org/10.13031/2013.23322

Hu J, Zhao L, Luo J, Gong H, Zhu N (2022) A sustainable reuse strategy of converting waste activated sludge into biochar for contaminants removal from water: modifications, applications and perspectives. J Hazard Mater 438:129437. https://doi.org/10.1016/j.jhazmat.2022.129437

Huang GG, Liu YF, Wu XX, Cai JJ (2019) Activated carbons prepared by the KOH activation of a hydrochar from garlic peel and their CO2 adsorption performance. New Carbon Mater 34:247–257. https://doi.org/10.1016/S1872-5805(19)60014-4

Ip A, Barford J, McKay G (2008) Production and comparison of high surface area bamboo derived active carbons. Bioresour Technol 99:8909–8916. https://doi.org/10.1016/j.biortech.2008.04.076

Jribi S, Miyazaki T, Saha BB, Pal A, Younes MM, Koyama S, Maalej A (2017) Equilibrium and kinetics of CO2 adsorption onto activated carbon. Int J Heat Mass Transf 108:1941–1946. https://doi.org/10.1016/j.ijheatmasstransfer.2016.12.114

Kan Y, Li J, Zhang S, Gao Z (2023) Novel bridge assistance strategy for tailoring crosslinking networks within soybean-meal-based biocomposites to balance mechanical and biodegradation properties. Chem Eng J 472:144858. https://doi.org/10.1016/j.cej.2023.144858

Li H, Li G, Li L (2023a) Comparative investigation on combustion characteristics of ADN-based liquid propellants in inert gas and oxidizing gas atmospheres with resistive ignition method. Fuel 334:126742. https://doi.org/10.1016/j.fuel.2022.126742

Li M, Xia Q, Lv S, Tong J, Wang Z, Nie Q, Yang J (2022) Enhanced CO2 capture for photosynthetic lycopene production in engineered Rhodopseudomonas palustris, a purple nonsulfur bacterium. Green Chem 24(19):7500–7518. https://doi.org/10.1039/d2gc02467e

Li S, Han K, Li J, Li M, Lu C (2017) Preparation and characterization of super activated carbon produced from gulfweed by KOH activation. Microporous Mesoporous Mater 243:291–300. https://doi.org/10.1016/j.micromeso.2017.02.052

Li X, Wang F, Al-Razgan M, MahrousAwwad E, ZilolaAbduvaxitovna S, Li Z, Li J (2023b) Race to environmental sustainability: Can structural change, economic expansion and natural resource consumption effect environmental sustainability? A novel dynamic ARDL simulations approach. Resour Policy 86:104044. https://doi.org/10.1016/j.resourpol.2023.104044

Liang Y, Li J, Xue Y, Tan T, Jiang Z, He Y, Shangguan W, Yang J, Pan Y (2021) Benzene decomposition by non-thermal plasma: a detailed mechanism study by synchrotron radiation photoionization mass spectrometry and theoretical calculations. J Hazard Mater 420:126584. https://doi.org/10.1016/j.jhazmat.2021.126584

Liu J, Li H, Harvey J, Airey G, Lin S, Lee SLJ, Zhou Y, Yang B (2023) Study on leaching characteristics and biotoxicity of porous asphalt with biochar fillers. Transp Res D Transp Environ 122:103855. https://doi.org/10.1016/j.trd.2023.103855

Liu L, Tang Y, Liu D (2022) Investigation of future low-carbon and zero-carbon fuels for marine engines from the view of thermal efficiency. Energy Rep 8:6150–6160. https://doi.org/10.1016/j.egyr.2022.04.058

Lu S, Guo J, Liu S, Yang B, Liu M, Yin L, Zheng W (2022) An improved algorithm of drift compensation for olfactory sensors. Appl Sci 12(19):9529. https://doi.org/10.3390/app12199529

Lua AC, Yang T, Guo J (2004) Effects of pyrolysis conditions on the properties of activated carbons prepared from pistachio-nut shells. J Anal Appl Pyrolysis 72:279–287. https://doi.org/10.1016/j.jaap.2004.08.001

Mahapatra K, Ramteke D, Paliwal L (2012) Production of activated carbon from sludge of food processing industry under controlled pyrolysis and its application for methylene blue removal. J Anal Appl Pyrolysis 95:79–86. https://doi.org/10.1016/j.jaap.2012.01.009

Malik R, Ramteke D, Wate S (2007) Adsorption of malachite green on groundnut shell waste based powdered activated carbon. Waste Manage 27:1129–1138. https://doi.org/10.1016/j.wasman.2006.06.009

Maniarasu R, Rathore SK, Murugan S (2022) Preparation, characterization, and performance of activated carbon for CO_2 adsorption from CI engine exhaust. Greenh Gases Sci Technol 12(2):284–304. https://doi.org/10.1002/ghg.2145

Medhat A, El-Maghrabi HH, Abdelghany A, Menem NMA, Raynaud P, Moustafa YM, Elsayed MA, Neda AA (2021) Efficiently activated carbons from corn cob for methylene blue adsorption. Appl Surf Sci Adv 3:100037. https://doi.org/10.1016/j.apsadv.2020.100037

Mohammadi N, Mousazadeh B, Hamoule T (2021) Synthesis and characterization of NH 2-SiO 2@ Cu-MOF as a high-performance adsorbent for Pb ion removal from water environment. Environ Dev Sustain 23:1688–1705. https://doi.org/10.1007/s10668-020-00646-9

Mousazadeh B, Mohammadi N, Hamoule T (2021) Removal of phosphate from the aqueous environment using iron oxide/activated carbon composites: activated carbon derived from ziziphus nuts as a new precursor. Iran J Chem Eng 18:52–62. https://doi.org/10.1016/j.apsadv.2020.100037

Nagarajan L, Kumaraguru K, Saravanan P, Rajeshkannan P, Rajasimman M (2022) Facile synthesis and characterization of microporous-structured activated carbon from agro waste materials and its application for CO_2 capture. Environ Tech 43:3983–3992. https://doi.org/10.1080/09593330.2021.1938243

Nahil MA, Williams PT (2012) Pore characteristics of activated carbons from the phosphoric acid chemical activation of cotton stalks. Biomass Bioenergy 37:142–149. https://doi.org/10.1016/j.biombioe.2011.12.019

Oginni O, Singh K, Oporto G, Dawson-Andoh B, McDonald L, Sabolsky E (2019) Influence of one-step and two-step KOH activation on activated carbon characteristics. Bioresour Technol Rep 7:100266. https://doi.org/10.1016/j.biteb.2019.100266

Osasona I, Aiyedatiwa K, Johnson J, Faboya OL (2018) Activated carbon from spent brewery barley husks for cadmium ion adsorption from aqueous solution. Indones J Chem 18:145–152. https://doi.org/10.22146/ijc.22422

Ozdemir I, Şahin M, Orhan R, Erdem M (2014) Preparation and characterization of activated carbon from grape stalk by zinc chloride activation. Fuel Process Technol 125:200–206. https://doi.org/10.1016/j.fuproc.2014.04.002

Parshetti GK, Chowdhury S, Balasubramanian R (2015) Biomass derived low-cost microporous adsorbents for efficient CO_2 capture. Fuel 148:246–254. https://doi.org/10.1016/j.fuel.2015.01.032

Plaza MG, Pevida C, Arias B, Casal M, Martín C, Fermoso J, Rubiera F, Pis J (2009) Different approaches for the development of low-cost CO_2 adsorbents. J Environ Eng 135:426–432

Ramesh T, Jafri RI, Reddy NP, Raveendra NV, Rajalakshmi N, Dhathathreyan KS, Tamilarasan P, Ramaprabhu S (2018) Sustainable porous carbon derived from cotton for high

power supercapacitor and CO_2 storage applications. Adv Porous Mater 6:8–18. https://doi.org/10.1166/apm.2018.1153

Raut ER, Bedmohata MA, Chaudhari AR (2022) Comparative study of preparation and characterization of activated carbon obtained from sugarcane bagasse and rice husk by using H3PO4 and ZnCl2. Mater Today: Proc 66:1875–1884

Ravi M, Rathore SK, Sivalignam M (2022) Experimental investigation on using adsorbent for post-combustion carbon dioxide capture from CI engine exhaust. Environ Prog Sustain 41(6):e13987. https://doi.org/10.1002/ep.13987

Roosta M, Ghaedi M, Daneshfar A, Darafarin S, Sahraei R, Purkait M (2014) Simultaneous ultrasound-assisted removal of sunset yellow and erythrosine by ZnS: Ni nanoparticles loaded on activated carbon: optimization by central composite design. Ultrason Sonochem 21:1441–1450. https://doi.org/10.1016/j.ultsonch.2014.01.018

Serafin J, Sreńscek-Nazzal J, Kamińska A, Paszkiewicz O, Michalkiewicz B (2022) Management of surgical mask waste to activated carbons for CO_2 capture. J CO2 Util 59:101970. https://doi.org/10.1016/j.jcou.2022.101970

Shafeeyan MS, Daud WMAW, Houshmand A, Shamiri A (2010) A review on surface modification of activated carbon for carbon dioxide adsorption. J Anal Appl Pyrolysis 89:143–151. https://doi.org/10.1016/j.jaap.2010.07.006

Tan Z, Chen G, Zhu Y (2015) Carbon-based supercapacitors produced by the activation of graphene. Nanocarbons Adv Energ Stor. https://doi.org/10.1002/9783527680054.ch7

Thue PS, dos Reis GS, Lima EC, Sieliechi JM, Dotto G, Wamba AG, Dias SL, Pavan FA (2017) Activated carbon obtained from sapelli wood sawdust by microwave heating for o-cresol adsorption. Res Chem Intermed 43:1063–1087. https://doi.org/10.1007/s11164-016-2683-8

Tian H, Li R, Salah B, Thinh P (2023) Bi-objective optimization and environmental assessment of SOFC-based cogeneration system: performance evaluation with various organic fluids. Process Saf Environ Prot 178:311–330. https://doi.org/10.1016/j.psep.2023.07.040

Toprak A, Kopac T (2017) Carbon dioxide adsorption using high surface area activated carbons from local coals modified by KOH, NaOH and ZnCl2 agents. Int J Chem React Eng. https://doi.org/10.1515/ijcre-2016-0042

Wang B, Gupta R, Bei L, Wan Q, Sun L (2023) A review on gasification of municipal solid waste (MSW): Syngas production, tar formation, mineral transformation and industrial challenges. Int J Hydrog Energy. https://doi.org/10.1016/j.ijhydene.2023.03.086

Wang C, Liu T (2017) Nori-based N, O, S, Cl co-doped carbon materials by chemical activation of ZnCl2 for supercapacitor. J Alloys Compd 696:42–50. https://doi.org/10.1016/j.jallcom.2016.11.206

Wang J, Heerwig A, Lohe MR, Oschatz M, Borchardt L, Kaskel S (2012) Fungi-based porous carbons for CO_2 adsorption and separation. J Mater Chem 22:13911–13913. https://doi.org/10.1039/C2JM32139D

Yahya MA, Al-Qodah Z, Ngah CZ (2015) Agricultural bio-waste materials as potential sustainable precursors used for activated carbon production: a review. Renew Sustain Energ Rev 46:218–235. https://doi.org/10.1016/j.rser.2015.02.051

Yakout S, El-Deen GS (2016) Characterization of activated carbon prepared by phosphoric acid activation of olive stones. Arab J Chem 9:S1155–S1162. https://doi.org/10.1016/j.arabjc.2011.12.002

Yokoyama TCJ, Cazetta AL, Bedin KC, Spessato L, Fonseca JM, Carraro PS, Ronix A, Silva MC, Silva TL, Almeida VC (2019) Stevia residue as new precursor of CO2-activated carbon: optimization of preparation condition and adsorption study of

triclosan. Ecotoxicol Environ Saf 172:403–410. https://doi.org/10.1016/j.ecoenv.2019.01.096

Yuan J, Li Y, Shan Y, Tong H, Zhao J (2023) Effect of magnesium ions on the mechanical properties of soil reinforced by microbially induced carbonate precipitation. J Mater Civ Eng 35(11):4023413. https://doi.org/10.1061/JMCEE7.MTENG-15080

Zhang G, Zhao Z, Zhu Y (2020) Changes in abiotic dissipation rates and bound fractions of antibiotics in biochar-amended soil. J Clean Prod 256:120314. https://doi.org/10.1016/j.jclepro.2020.120314

Zhang G, Zhao Z, Yin X, Zhu Y (2021) Impacts of biochars on bacterial community shifts and biodegradation of antibiotics in an agricultural soil during short-term incubation. Sci Total Environ 771:144751. https://doi.org/10.1016/j.scitotenv.2020.144751

Zeng H, Wang L, Zhang D, Yan P, Nie J, Sharma VK, Wang C (2019) Highly efficient and selective removal of mercury ions using hyperbranched polyethylenimine functionalized carboxymethyl chitosan composite adsorbent. Chem Eng J 358:253–263. https://doi.org/10.1016/j.cej.2018.10.001

Zhang Q, Gao S, Guo Y, Wang H, Wei J, Su X, Zhang H, Liu Z, Wang J (2023a) Designing covalent organic frameworks with Co-O4 atomic sites for efficient CO2 photoreduction. Nat Commun 14(1):1147. https://doi.org/10.1038/s41467-023-36779-4

Zhang X, Li C, Zhou Z, Liu B, Zhang Y, Yang M, Gao T, Liu M, Zhang N, Said Z, Sharma S, Ali HM (2023b) Vegetable oil-based nanolubricants in machining: from physicochemical properties to application. Chin J Mech Eng 36:76. https://doi.org/10.1186/s10033-023-00895-5

Zheng Y, Wang A (2010) Removal of heavy metals using polyvinyl alcohol semi-IPN poly (acrylic acid)/tourmaline composite optimized with response surface methodology. Chem Eng J 162:186–193. https://doi.org/10.1016/j.cej.2010.05.027

Authors and Affiliations

B. Mousazadeh[1] · N. Mohammadi[1] · M. R. Khosravi-Nikou[1]

✉ M. R. Khosravi-Nikou
mr.khosravi@put.ac.ir

[1] Gas Engineering Department, Petroleum University of Technology, Ahvaz, Iran